Synergistic effect of Gemcitabin-loaded metal organic frameworks nanoparticles with particle therapy

Pauline Maury, Ryoichi Hirayama, Xue Li, Pierre Mahou, Erika Porcel, Marie-Claire Schanne-Klein, Sandrine Lacombe, Ruxandra Gref, Erika Porcel

International Journal of Pharmaceutics 665 (2024) 124721

Contents lists available at ScienceDirect

International Journal of Pharmaceutics

journal homepage: www.elsevier.com/locate/ijpharm

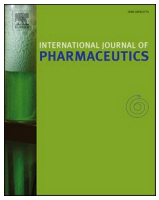

Synergistic effect of Gemcitabin-loaded metal organic frameworks nanoparticles with particle therapy

Pauline Maury [a,d,e], Ryoichi Hirayama [b], Xue Li [a], Pierre Mahou [c], Marie-Claire Schanne-Klein [c], Sandrine Lacombe [a], Ruxandra Gref [a], Erika Porcel [a,*]

[a] Université Paris Saclay, CNRS, Institut des Sciences Moléculaires d'Orsay (ISMO), 91405 Orsay, France
[b] Department of Charged Particle Therapy Research, QST Hospital, National Institutes for Quantum Science and Technology (QST), Chiba, Japan
[c] Laboratoire d'Optique et Biosciences (LOB), Ecole Polytechnique, CNRS, INSERM, Institut Polytechnique de Paris, Palaiseau, France
[d] Université Paris-Saclay, Gustave Roussy, Inserm U1030, Radiothérapie Moléculaire et Innovation Thérapeutique, F-94800, Villejuif, France
[e] Gustave Roussy, Département de radiothérapie, F-94800, Villejuif, France

ARTICLE INFO

Keywords:
Nanoparticles
Radiations
Hypoxia
Particle therapy
MOFs
3D cell model
Drug delivery

ABSTRACT

Combination of nanoagents with radiations has opened up new perspectives in cancer treatment, improving both tumor diagnosis and therapeutic index. This work presents the first investigation of an innovative strategy that combines porous metal–organic frameworks (nanoMOFs) loaded with the anti-cancer drug Gemcitabine monophosphate (GemMP) and particle therapy-a globally emerging technique that offers more precise radiation targeting and enhanced biological efficacy compared to conventional radiotherapy. This radiochemotherapy has been confronted with two major obstacles limiting the efficacy of therapeutics when tested *in vivo*: (i) the presence of hypoxia, one of the most important causes for radiotherapy failure and (ii) the presence of a microenvironment, main biological barrier to the direct penetration of nanoparticles into cancer cells.

On the one hand, this study explore the effects of hypoxia on drug delivery systems in combination with radiation, demonstrating that GemMP-loaded nanoMOFs significantly enhance the anticancer efficacy of particle therapy under both normoxic (pO_2 = 20 %) and hypoxic (pO_2 = 0.5 %) conditions. Notably, the presence of GemMP-loaded nanoMOFs allows the irradiation dose to be reduced by 1.4-fold in normoxia and at least 1.6-fold in hypoxia, achieving the same cytotoxic effect (SF=10 %) as carbon or helium ions alone. Synergistic effects between GemMP-loaded nanoMOFs and radiations have been observed and quantified. On the other hand, we also highlighted the ability of the nanoMOFs to diffuse through an extracellular matrix and accumulate in cells. An higher effect of the encapsulated GemMP than the free drug was observed, confirming the key role of the nanoMOFs in transporting the active substance to the cancer cells as a Trojan horse. This paves the way to the design of "all-in-one" nanodrugs where each component plays a role in the optimization of cancer therapy to maximize cytotoxic effects on hypoxic tumor cells while minimizing toxicity on healthy tissue.

1. Introduction

The combination of chemotherapy with radiations treatments, called chemoradiation, is the standard of care for many solid cancers(Pauwels et al., 2003; Song et al., 2017). In comparison with other therapeutic alternatives, this strategy exhibits clinical benefits, such as organ preservation and improved tumoral control(Seiwert et al., 2007). The spatial cooperation between the locoregional action of the radiotherapy and the systemic properties of the chemotherapy reduces the risk of metastasis (Gordon Steel and Peckham, 1979). Gemcitabin (Gem) is an efficient radiosensitizer already used in clinic which exerts its cytotoxic effect by targeting DNA(Carmichael et al., 1995). The anticancer nucleoside analog Gem is a prodrug which needs to be converted by cellular kinases into the pharmacologically active triphosphate form. However, in some cases, this intracellular conversion is not efficient leading to drug resistance and systemic toxicity. The direct administration of the phosphorylated form of Gem is hampered by its poor stability in biological media, low intracellular penetration and low tissue specificity(Bouffard et al., 1993).

A promising approach was proposed by Gref and coworkers to

* Corresponding author.
E-mail address: erika.porcel@universite-paris-saclay.fr (E. Porcel).

https://doi.org/10.1016/j.ijpharm.2024.124721
Received 13 June 2024; Received in revised form 11 September 2024; Accepted 13 September 2024
Available online 16 September 2024

improve the stability and intracellular delivery of Gem to tumor cells (Rodriguez-Ruiz et al., 2015). It consists in encapsulating with high efficiency the phosphorylated form of Gem, Gem-monophosphate (GemMP), in highly porous hybrid metal–organic nanoparticles (nanoMOFs). Encapsulated GemMP is then released to the target after a progressive degradation of nanoMOFs by the phosphates contained in the biological medium(Li et al., 2020; Simon-Yarza et al., 2017). These biodegradable(Li et al., 2017) and biocompatible(Baati et al., 2013) nanoparticles (NPs) protect the drug against degradation and significantly improve drug delivery in tumor cells(Ding et al., 2022). An important advantage of iron-based nanoMOFs, such as MIL-100(Fe) (MIL stands for Material of Institute Lavoisier), is their ability to enhance the effects of radiation(Li et al., 2020b). Additionally, these nanoMOFs possess intrinsic properties as contrast agents for MRI, making them multifunctional tools in cancer therapy(Horcajada et al., 2010).

Our group already reported the efficiency of GemMP-loaded nanoMOFs to improve the effect of radiations. This proof of concept was performed under normal incubator conditions, i.e. normoxic ($pO_2 = 20$ %) using monolayer cell cultures(Li et al., 2020). An 80 % increase of cell killing was observed when cells were exposed to gamma radiation (Cs-137, energy = 662 keV (γ)). This increase was among the strongest ever reported for tumor treatment with gamma irradiation and nanoparticles (NPs).

In response to the challenge of radioresistant cancers, our new study evaluates the effectiveness of combining these nanoagents with a more promising irradiation technique than conventional radiotherapy: particle therapy. This approach uses high-energy charged particles (carbon or helium ions of MeV/u) for highly targeted energy deposition, with maximum impact at the end of the particle trajectory (Bragg peak), thereby minimizing damage beyond the tumor and sparing surrounding healthy tissues (Porcel et al., 2014).

Compared to photons, charged particle beams exhibit greater biological effectiveness, inducing more complex DNA damage, including multiple damage sites or clustered lesions that enhance tumor cell destruction(Durante and Cucinotta, 2008; Durante et al., 2017; Hagiwara et al., 2019, 2017; Lorat et al., 2015; Nakano et al., 2022; Sage and Shikazono, 2017). Consequently, particle therapy is emerging as a preferred technique for treating tumors located near critical structures or organs, in patients where minimizing radiation dose is paramount, or for radioresistant tumors that are refractory to conventional treatments. In this perspective, treatment plans based on the use of carbon and helium ions appear particularly promising to exploit relative biological effectiveness and the dose reduction distal to the tumor(Graeff et al., 2018; Mazzucconi et al., 2018; Volz et al., 2020).

Radio-resistant tumors are mostly composed of hypoxic cells (oxygen concentration below 1 %) at the origin of poor treatment outcomes, high probability of relapse and increased risks of metastases(Brown and Wilson, 2004; McKeown, 2014; Vaupel and Mayer, 2007). This pathological phenomenon occurs because tumor cells consume more oxygen than the blood supply can provide, due to their high metabolism, disorganized vasculature, and limited oxygen diffusion.

The primary objective of this work was to evaluate the impact of hypoxia on the efficiency of GemMP-loaded nanoMOFs when combined with radiation, by monitoring oxygen concentration in cells under both normoxic and hypoxic conditions using 2D HeLa cell cultures.

On the other hand, the microenvironment often compromises the antitumor efficiency of the treatments *in vivo* (Jain, 1997; Minchinton et al., 2006; Tchoryk et al., 2019). In tumors, cells interact with and through an extracellular matrix (ECM), structural and biochemical support, which can constitute an obstacle to the penetration and the accumulation of nanoagents in solid tumors after extravasation from the blood vessels. It was reported that the ECM natural barrier can disrupt the cells' response both to a variety of nanoagents such as metallic NPs and to irradiation(Goodman et al., 2007; Li et al., 2022; Magzoub et al., 2008; Minchinton and Steichen et al., 2013; Tannock, 2006; Netti et al., 2000). The cellular uptake and penetration in tumors is strongly dependent on NPs characteristics such as size, shape, surface charge, surface properties, and chemical composition (Tchoryk et al., 2019). The other objective of the work was to study if ECM limits nanoMOFs diffusion and hampers the effect of irradiation. To mimic the tumor environment, a realistic 3D cell model was set up and a comparison of the effects produced on cells in 2D cultures or embedded in a collagen I matrix was conducted.

2. Materials

2.1. Materials

Iron (III) chloride hexahydrate (98 %) was purchased from Alfa Aesar (Schiltigheim, France). 1,3,5-benzenetricarboxylic acid (BTC, 95 %) and absolute ethanol (99 %) were from Sigma-Aldrich (Saint-Quentin-Fallavier, France). These materials were used for the synthesis of nanoMOFs. 20,20- difluorodeoxyxytidine monophosphate (Gem-MP) from Toronto research Chemicals (North York, Canada) was the drug used in this study.

2.2. NanoMOFs synthesis and Gem incorporation

The synthesis and characterization of nanoMOFs loaded with GemMP have been the subject of a previous publication (Li et al., 2020). Synthesis of iron trimesate MIL-100(Fe) nanoMOFs (MIL stands for Material of Institute Lavoisier) was performed by microwave-assisted solvent-free "green" hydrothermal techniques as previously described[13]. Briefly, a mixture of iron chloride (8.97 mmol) and trimesic acid (4.02 mmol) in 20 mL of deionized water was placed in Pyrex reactors and heated for 6 min at 130 °C under stirring. The applied power was 1600 Watts (Mars-5, CEM, US). The reactors were cooled in ice bath and the synthesized nanoMOFs were recovered by centrifugation (10,000*g*, 15 min) and were purified by washing with absolute EtOH six times to remove the residual non-reacted trimesic acid. The nanoMOFs were stored in EtOH until final use. GemMP was incorporated by coordination with the accessible unsaturated sites of Fe trimers. Encapsulation efficacy was close to 100 %, for a drug loading of GemMP in nanoMOFs of 5 wt% ensuring a loading of these frameworks without size modification (220 ± 25 nm & 226 ± 28 nm before and after GemMP encapsulation (Li et al., 2020a). TEM images of nanoMOFs empty or loaded with 5 % Gem MP are provided in the Supplementary section (Supplementary Material, 'NanoMOFs synthesis and GemMP incorporation'). For microscopy studies, the nanoMOFs (0.5 mg/mL) were labelled with the fluorescent tags Rhodamine B or Alexa 568. After an overnight incubation (GemMP:nanoMOF weight ratio of 1:10), the free fluorophores were eliminated by successive water washing as previously reported(Li et al., 2020). Further details on nanoagents characterization are provided in the supplementary section.

2.3. Cell cultures

The experiments were performed with the human cervical adenocarcinoma cell line (HeLa), purchased from RIKEN. Cells were cultivated in Eagle's Modified Eagle Medium (E-MEM) supplemented with 10 % heat-inactivated foetal bovine serum (FBS), 1 % penicillin/streptomycin (P/S) and 1 % L-glutamine (Life Technologies). 2D experiments were performed from monolayer cultures of Hela cultured in flasks while 3D cell collagen based models (3D-CCMs) were prepared by embedding ~ 350 000 HeLa cells in a collagen I matrix using a commercially available system (RAFT™ 3D cell culture kit, Lonza, Basel, Switzerland). As detailed in a previous study(Maury et al., 2021), 3D-CCMs were prepared by mixing a cell suspension of 2.4–2.6 cells/mL with 10X MEM, neutralizing solution and 2 mg/mL rat-tail type I collagen solution. 320 μL of the final solution were dispensed in each 96 well plate and kept in the incubator for 15 min. RAFT™ absorbers were finally disposed on top

of each well for 15 min.

3. Methods

3.1. Toxicity of nanoagents

Monolayer cells were incubated with these concentrations for 6 h while 3D-CCMs were incubated during 18 h to allow homogeneous migration of the agents in the matrix. 2D toxicity studies were performed from the control samples of the clonogenic assay (see section 3.4.4 for detailed protocol). Toxicity of GemMP-loaded nanoMOFs for cells embedded in the 3D-CCMs were determined for a concentration equivalent to the 2D study (i.e. 17 μg/mL of nanoMOFs loaded with 0.85 μg/mL of GemMP) using an MTT test. In this purpose, 3D-CCMs were exposed to 125 μL of tetrazolium dye MTT 3-(4,5-dimethylthiazol-2-yl)-2,5-diphenyltetrazolium bromide in a 96-well plate at 37 °C for 4 h. Then, 125 μL of lysis buffer was added to dissolve the formazan crystals. The proportion of living and metabolically active cells, was quantified from the absorbance measured with a Glomax® Microplate reader (Promega©) (absorbance 560 nm). A sample consisting of 3D-CCM incubated with a volume of water equivalent to the volume of GemMP-loaded nanoMOFs was used as positive control. A sample composed of 3D-CCM treated for 4 h with 200 μL of menadione (500 μmol/L) was used as negative control.

3.2. Localisation of nanoagents

The localisation of the nanoMOFs in cells was characterized using two techniques of fluorescence microscopy, namely confocal and multiphoton microscopies for the 2D and 3D samples, respectively.

3.2.1. Confocal microscopy protocol (for the 2D cultures)

Monolayer living cells incubated with nanoMOFs labelled with Adamantane-Rhodamine for 6 h were imaged on sterile glass slides using a LEICA SP5 confocal system according to the protocol described in our previous study(Li et al., 2020). Briefly, the images were acquired at 514 nm excitation wavelength, in the 560 to 600 nm range of emission. During the acquisition, the temperature was kept at 37 °C and the CO_2 was regulated at 5 %.

3.2.2. Multiphoton microscopy protocol (for the 3D samples)

Multiphoton microscopy was used to study the nanoMOFs migration in 3D-CCMs. 3D-CCMs were incubated with nanoMOFs-Alexa 568 in the conditions specified above (i.e. 17 μg/mL nanoMOFs concentration, 18 h incubation time). After PBS washing, nuclei were stained for 20 min with 1 μmol/L Hoescht 33,342 solution. 3D multimodal multiphoton images were recorded with a commercial multiphoton microscope (TriM Scope II, LaVision BioTec), using an objective lens (25 × 1.05NA, XLPLN25XWMP2, Olympus). Collagen of the 3D-CCMs was imaged without any labelling by taking advantage of its intrinsic second harmonic generation (SHG) signal. Excitation was provided by an ultrafast oscillator (Insight DeepSee, Spectraphysics) set at $\lambda = 1140$ nm. The SHG signal at 570 nm was collected in the forward direction by a condenser (U-AAC achromatic aplanatic condenser 1.40NA, Olympus), separated from the laser by a dichroic mirror (Di02-R635, Semrock), selected with an interference filter (FF02-575–25, Semrock) and detected by a photomultiplier tube (H7422-40, Hamamatsu). Cell nuclei and nanoMOFs were imaged simultaneously using a common excitation at $\lambda = 830$ nm by a second ultrafast oscillator (Mai Tai HP DeepSee, Spectraphysics). The two-photon excitation fluorescence (2PEF) signals were collected in epidetection with the microscope objective and a dichroic mirror (T695lpxr, Chroma). The signals were then split in two using a dichroic mirror (FF495-Di03, Semrock), selected with interference filters (FF01-450–70 or FF01-466–40 for the cell nuclei labelled with Hoescht 33,342 and FF01-607–70 for the nanoMOFs labelled with Alexa 568 – Semrock) and detected by photomultiplier tubes (H6780-01 and H7422-40, Hamamatsu). Data acquisition was performed on a 350 μm square field of view with a pixel size of 0.192 μm and an acquisition frequency of 400 Hz. 3D images were captured with a z-step of 1 μm.

3.3. Quantification of nanoagents

The method used to quantify the nanoMOFs concentration in cells of 2D cultures is described elsewhere (Li et al., 2020). Briefly, the intracellular amount of nanoMOFs was determined using a method based on iron staining with potassium ferrocyanide(Wuttke et al., 2015). Although reliable, this method is time-consuming as it requires the establishment of a calibration curve. So, the quantification of the nanoMOFs concentrations contained in (i) entire 3D-CCM and (ii) in the 295 680 cells extracted from the 3D-CCM, was performed by faster method, the Inductively Coupled Plasma-Mass Spectroscopy (ICP-MS) (UT2A – Technological Center, Pau, France). To collect the cells from the 3D-CCMs, an addition step of enzymatic degradation with 1 mg/mL collagenase from Clostridium histolyticum (Sigma-Aldrich©) was needed.

3.4. Irradiation experiments

3.4.1. Preparation of 2D samples to study the influence of oxygen influence on irradiation effects

Around 200 000 cells per sample were prepared onto 3.8 cm glass dishes 24 h prior to irradiation. The cells were incubated 6 h before irradiation with the agents at respective concentrations in the solution (17 μg/mL nanoMOFs, 0.85 μg/mL GemMP and 17 μg/mL of nanoMOFs containing 0.85 μg/mL of GemMP). After 5 h, the volume of the medium was reduced from 3 mL down to 0.9 mL. For the experiments performed with hypoxic conditions (setup environment composed of approximately 0.5 % O_2, 94.5 % N_2 and 5 % CO_2, respectively), the samples were disposed 1 h prior to irradiation in a gas chamber flushed with a mixture of N_2/CO_2/air of 950/50/25 mL/min respectively to reach the required oxygen concentration. For normoxic conditions, the dishes were placed in the radiation chamber under atmospheric conditions (20 % O_2) 30 min before irradiation.

3.4.2. Preparation of 3D samples to study the influence of the matrix on irradiation

3D-CCMs were prepared in 96 wells plates 24h before irradiation (see 2.1.2). 18 h before irradiation, 3D-CCMs were put in contact with solution of free drug or nanoMOF formulation containing equivalent amounts of GemMP and empty nanoMOFs as controls. Incubation concentrations were the same as for 2D experiments (i.e. 17 μg/mL nanoMOFs, 0.85 μg/mL GemMP and 17 μg/mL of nanoMOFs containing 0.85 μg/mL of GemMP). Samples were incubated at 37 °C until irradiation. Just before irradiation, these solutions were replaced by fresh cell culture medium. After irradiation, the cells were extracted from the 3D-CCM matrix using 1 mg/mL collagenase as indicated in a previous study(Maury et al., 2021).

3.4.3. Irradiations

The irradiations were performed using passive beam delivery systems at the Heavy Ion Medical Accelerator in Chiba (HIMAC), QST, Chiba, Japan(Porcel et al., 2014). Two 10 cm diameter beams of different LET were used: a beam of carbon ions, $^{12}C^{6+}$ (initial energy = 290 MeV/u, LET_d = 50 keV/μm) and a beam of helium ions, $^{4}He^{2+}$ (initial energy = 150 MeV/u, LET_d = 12 keV/μm). Dishes were irradiated vertically and one by one, at the center of a 6 cm-SOBP (spread-out Bragg peak) with a dose rate of 3 Gy/min.

3.4.4. Analysis by clonogenic assay

The effects of radiation combined with nanoagents was analyzed by clonogenic assay as described elsewhere(Maury et al., 2021). Briefly, harvested cells were seeded in Petri dishes to determine the ability of

cells to proliferate and form colonies. For each condition, cell survival curves were established and simulated with a linear-quadratic model (LQ) as commonly used.

3.4.5. Quantitative parameters of analysis

Statistical F-tests, based on a maximum likelihood (ML) method, were performed using the CFAssay package included in the R software (Braselmann, 2019; Braselmann et al., 2015). They allow concluding about the significance of the difference observed:

i. between the cell survival curve of the control and those obtained in the presence of nanoagent (nanoMOFs, GemMP or GemMP-loaded nanoMOFs)
ii. between the curves with nanoMOFs alone or loaded with GemMP.

Statistical analysis was applied from the experimental points and significance of the p values was indicated on the survival curve as follows: 0 '***', 0.001 '**', 0.01 '*', 0.05 '.', 0.1 ' ', 1.

Efficiency of combined strategies was quantified calculating the dose enhancement factor (DEF) which is the ratio between the radiation dose needed to achieve a surviving fraction of 10 % in the control and the radiation dose needed to obtain the same biological effect in the presence of nanoagents (Equation (1).

$$DEF_{SF=10\%} = \frac{D^{c}_{SF}}{D^{NP}_{SF}} \quad (1)$$

Hypoxia-induced radio-resistance was quantified by the oxygen enhancement ratio (OER). It is defined as the ratio between the dose of radiation needed when oxygen concentration is reduced (here pO_2 = 0.5 %) and the radiation dose required in fully oxygenated conditions (air, $pO_2 \sim 20$ %) to produce the same level of biological effect (here SF=10 %) (Equation (2). OER is related to indirect effects and thus to the quality of the beam (LET dependency).

$$OER = \frac{D^{SF}_{hypoxic}}{D^{SF}_{normoxic}} \quad (2)$$

To characterize the nature of the effects produced by combing the radiations with GemMP-loaded MOFs, an isobologram analysis was performed using the software CompuSyn(Chou and Martin, 2005). This method, introduced by Chou-Talalay(Chou, 2010; Chou et al., 1984), is based on the calculation of the combination index (CI) according to the Equation (3). The value of the CI determines the nature of the effects: antagonist when CI>1.0, additive for CI=1.0 or synergetic when CI<1.0 (Huang et al., 2019).

$$\boldsymbol{CI} = \frac{(\boldsymbol{D})_1}{(\boldsymbol{D_x})_1} + \frac{(\boldsymbol{D})_2}{(\boldsymbol{D_x})_2} \quad (3)$$

$(D_x)_1$ and $(D_x)_2$ are the doses that give a survival fraction (Fa) for the treatments of the cells by radiation only (labelized 1) or GemMP-loaded nanoMOFs alone (labelized 2). $(D)_1$ and $(D)_2$ are the doses that reproduce the same cytotoxic effect when a combination of nanoagents with radiation is used. Values of $(D_x)_1$ and $(D_x)_2$ are directly extracted from the median-effect equation of Chou (Equation (4) (Chou et al., 2010) where D_m is the median effect dose (e.g SF=50 %).

$$\boldsymbol{D_x} = \boldsymbol{D_m}\cdot\left(\frac{\boldsymbol{F_a}}{1-\boldsymbol{F_a}}\right)^{\frac{1}{m}} \quad (4)$$

D_m(more precisely $\log(D_m)$) is obtained from the x-intercept of the dose effect plot (linearization of the Equation (4) which is $y = \log(\frac{F_a}{1-F_a})$ function to $x = \log(D)$. m is the dynamic-order signifying the shape of the dose–effect curve where $m = 1$, >1, and < 1 indicate hyperbolic, sigmoidal, and flat sigmoidal, respectively. In this study, the cell fractions obtained at different doses for the treatments by (i) nanoagents alone (ii) radiation alone and (iii) nanoagents combined with radiation, were implemented in the CompuSyn. Median-Effect Plot was generated by the software, which also provides the values of m, D_m, $(D)_{1,2}$ and $(Dx)_{1,2}$ and finally the CI values.

4. Results

4.1. Toxicity of nanoagents

4.1.1. Toxicities for cells cultivated in 2D monolayers

In presence of empty nanoMOFs (17 μg/ mL), the surviving fraction of HeLa cells was higher than 95 %, indicating the absence of cytotoxicity, namely mitotic death, due to the nanoMOFs. In contrast, free GemMP or GemMP incorporated in nanoMOFs induced cytotoxicities that are similar and presented in Table 1. An equivalent GemMP concentration of ~ 1.7 μg/ mL (10 wt%) led to surviving fractions in monolayer cultures around 50–55 %, in accordance with our previous experiments(Li et al., 2020). The equivalent GemMP concentration of ~ 0.85 μg/ mL (5 wt%) resulted in a surviving fraction of 74 % for the free GemMP and 78 % for GemMP-loaded nanoMOFs. This last drug concentration was therefore chosen for the present study so in these conditions we considered both agents as non-toxic since the cell survival was over 70 %, in agreement with the international standard for biological evaluation of medical devices (ISO 10993–5:2009-Part 5).

4.1.2. Toxicities in cells embedded in 3D-CCMs

The toxicity of the working concentration of 0.85 μg/mL GemMP (free or encapsulated in nanoMOFs) was assessed for cells embedded in 3D-CCM. The Table 2 presents the survival fraction obtained for both conditions, without irradiation. The difference between the free GemMP and GemMP-loaded nanoMOFs doesn't appear significant. The MTT assay (Fig. 1B) showed that the concentration of 5 wt% GemMP loaded nanoMOFs was non-toxic for cells cultured in 3D. Mitochondrial activity of cells incubated with GemMP-loaded nanoMOFs (in black) was found identical to that of the control cells (in green), while results were significantly different from the negative control (in red).

4.2. Localisation of GemMP-loaded nanoMOFs in cells

In order to avoid interfering with the entrapped GemMP drug, empty nanoMOFs were surface-labelled with fluorescent dyes as previously described. Confocal images of nanoMOFs labelled with rhodamine B internalized in 2D cells are presented in Fig. 1a. NanoMOFs were found exclusively in the cytoplasm and not in the nuclei. Multiphoton microscopy images of nanoMOFs internalized in 3D-CCMs are presented in Fig. 1 b-c-d. For the first time, we observed that nanoMOFs can diffuse through the collagen matrix of 3D-CCM. After 18 h, they have infiltrated the entire sample in depth and are homogeneously distributed in the matrix. The nanoMOFs penetrated the cells and localized as clusters in the cytoplasm but not in the nuclei, as demonstrated in the case of 2D monolayers(Li et al., 2020).

4.3. Quantification of GemMP-loaded nanoMOFs in cells

The quantification of GemMP free nanoMOFs in 2D monolayers cultures was performed in a previous study where we showed that monolayer cells incubated with 17 μg/mL of empty nanoMOFs during 6 h internalized around 8 pg of nanoMOFs per cell.

In this work, we quantified GemMP free nanoMOFs in the 3D-CCMs

Table 1
Comparison of the surviving fractions of cells (2D monolayer) in the presence of GemMP (5 or 10 wt%), free or loaded in 17 μg/mL nanoMOFs.

Concentration in GemMP	SF for free GemMP	SF for GemMP-loaded nanoMOFs
1.70 μg/mL (10 wt%)	50 % ± 7 %	55 % ± 4 %
0.85 μg/mL (5 wt%)	**74 % ± 15 %**	**78 % ± 8 %**

Table 2
Comparison of the surviving fractions obtained on cells contained in the 3D-CCM in the presence of free GemMP (5 wt%) or GemMP loaded in nanoMOFs (17 μg/mL).

Concentration in GemMP	SF for free GemMP	SF for GemMP-loaded nanoMOFs
0.85 μg/mL (5 wt%)	**67.3 % ± 12.5 %**	**88.7 % ± 10.2 %**

(cells and collagen matrix). After 18 h of incubation, 1.7 μg – out of 4.08 μg of available nanoMOFs in the medium – penetrated in the 3D-CCMs. It corresponds to an uptake of 42 %. From this quantity, 0.74 μg (43.5 %) of nanoMOFs was internalized by the cells themselves. The rest (56.5 %) remained in the collagen matrix. In each cell, the amount of nanoMOFs is thus ~ 2.51 pg. The nanoagents used for the irradiation experiments were composed of 5 wt% GemMP-loaded nanoMOFs, which corresponds to ~ 0.125 pg of GemMP per cell in average.

4.4. Impact of nanoMOFs, GemMP and GemMP-loaded nanoMOFs on radiation effects – comparison of normoxic (pO_2 = 20 %) and hypoxic conditions (pO_2 = 0.5 %) (in 2D cell cultures)

4.4.1. Carbon irradiations

The normalized surviving curves obtained by the exposition of monolayer cultures with 290 MeV/u carbon ions beam (LET_d = 50 keV/μm) in normoxic conditions (pO_2 = 20 %) and hypoxic conditions (pO_2 = 0.5 %) are presented in Fig. 2. As expected, the survival fractions decrease with increasing the irradiation dose, following the LQ model. The addition of GemMP-free (not loaded) nanoMOFs do not amplify the radiation effect, in normoxic nor hypoxic conditions. On the other hand, the cell response to irradiation was strongly increased when cells were incubated with free GemMP or GemMP-loaded nanoMOFs. For the two oxygenation conditions, the surviving fraction at 2 Gy is reduced by more than 40 % (44 % and 57 % for GemMP and GemMP-loaded nanoMOFs, respectively). The DEF value is close to 1.4 in normoxia and 1.5—–1.6 in hypoxia (Table 3). The OER is lower when the cells are loaded with GemMP-loaded nanoMOFs, from 1.4 (control) to 1.2 (GemMP-loaded nanoMOFs) (Fig. 2C and D).

Combination indexes (CI) were calculated to determine the nature of the effects generated by the combination of irradiations with the nanoagents: antagonist (if CI>1.0), additive (if CI=1.0) or synergetic (if CI<1.0). For GemMP, the effect is synergetic when the irradiation dose > 1 Gy and additive below. With GemMP-loaded nanoMOFs, the effect is synergetic for all the doses and maximal at high radiation dose.

4.4.2. Helium irradiation

The survival curves obtained by the exposition of monolayer culture with 150 MeV/u helium ions beam (LET_d = 12 keV/μm, lower than carbon LET) are presented in Fig. 4. Similarly to carbon ions irradiation, nanoMOFs did not exhibit any effect cell on radiation response but the presence of GemMP induced a radio-sensitization of cells, in particular in hypoxic conditions. As observed before, the DEF values (Table 4) are similar for GemMP free and loaded in the nanoMOFs, which shows that the encapsulation of GemMP has no significant influence on the treatment efficiency. Here also, the OER decreases (from 1.6 to 1.3) in the presence of GemMP-loaded nanoMOFs (Fig. 3 C-D), showing that the effect of oxygen decreases.

For the same conditions of incubation (control, GemMP, free nanoMOFs or GemMP-loaded nanoMOFs), the cell survival fractions were systematically lower under carbon ions radiation as to compare with

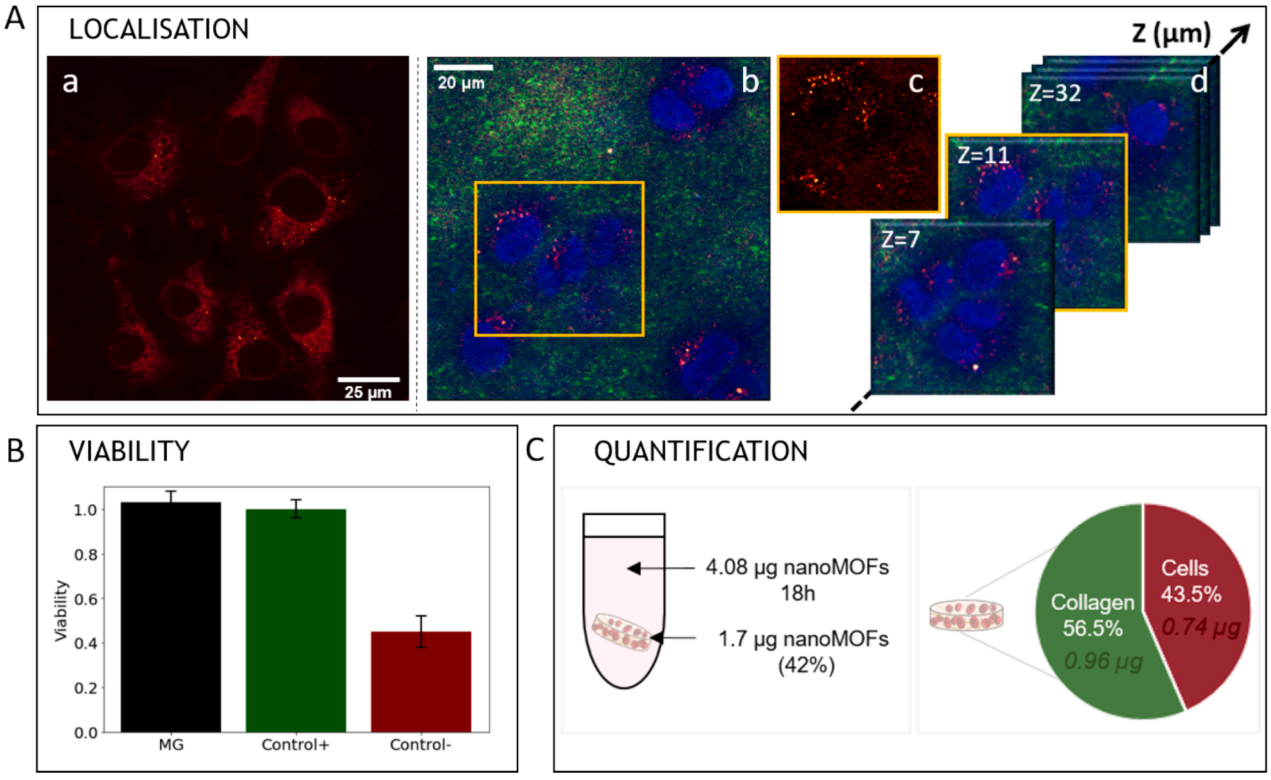

Fig. 1. (A) Localisation of nanoMOFs in (a) monolayer cultures after 6 h incubation (adapted from Li et al., 2020) (b-c-d) 3D-CCMs at different z-depths after 18 h incubation. 2PEF from nanoMOFs is depicted in red, SHG from collagen in green and 2PEF from nuclei in blue. The (b) and (c) images represent the same slice in the sample: (b) is the merged image (SHG+2PEF) while (c) represents the nanoparticle 2PEF channel in red exclusively. (d) corresponds to images (SHG+2PEF) of the area framed in orange in (b), performed at different depths (z). (B) Evaluation of the cytotoxicity of GemMP-loaded nanoMOFs (MG) based on the mitochondrial activity measurement of cells contained in 3D-CCM (in black) (absorbance at 560 nm) compared to positive control i.e. 3D-CCM without any treatment (green) and negative control i.e. 3D-CCM treated with menadione (red). (C) Quantification of nanoMOFs available in the incubation medium and internalized in 3D-CCMs after 18 h. The internalized nanoMOFs are found in the collagen or in the cells according to the distribution shown in the diagram.

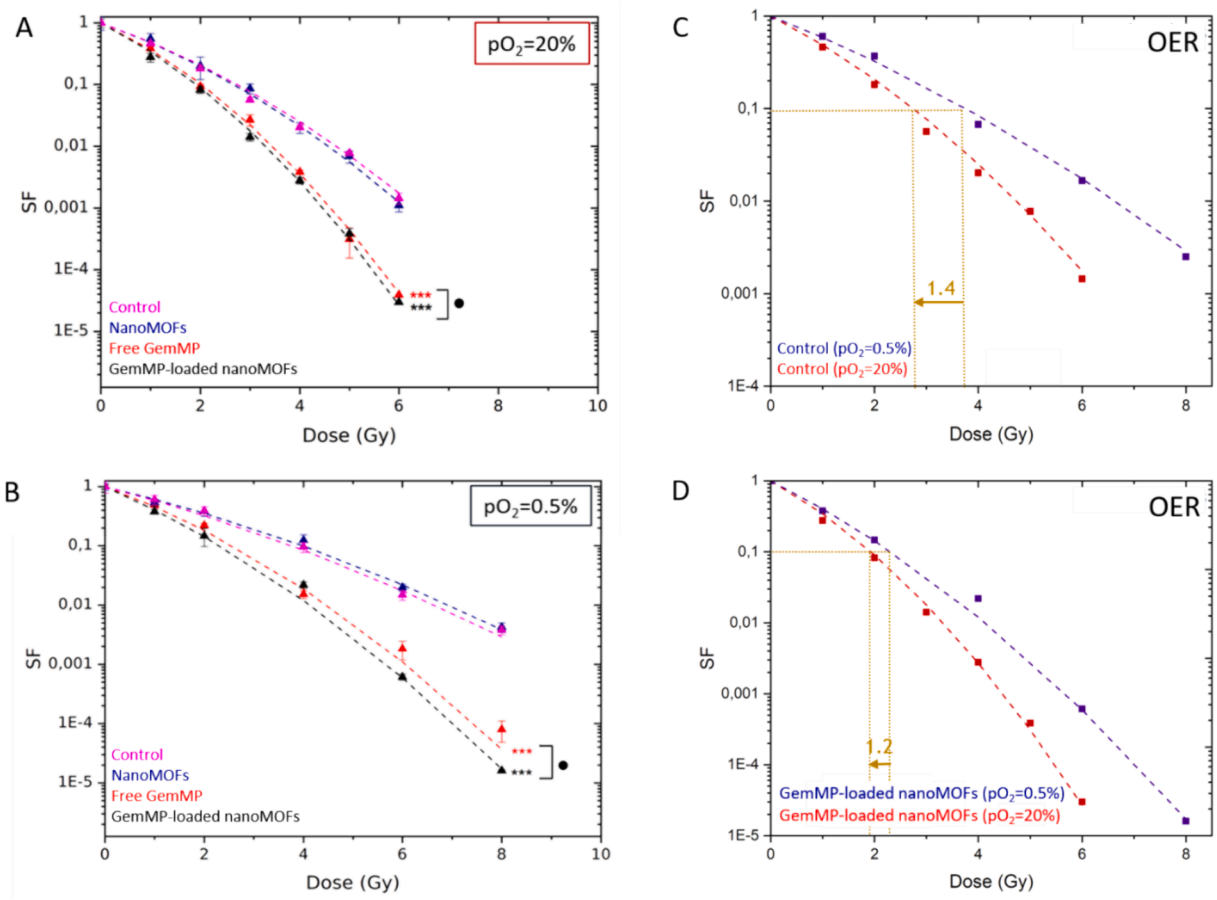

Fig. 2. Survival curves obtained with 290 MeV/u carbon ions irradiation (LETd = 50 keV/μm) in (A) normoxic and (B) hypoxic conditions. Differences between the control and GemMP or GemMP-loaded nanoMOFs are significant (p values < 0.001 (***)), but not significant between GemMP and GemMP-loaded nanoMOFs (p value < 0.1 (.)) Oxygen effect for cells without nanoagents (C) and cells incubated with GemMP-loaded nanoMOFs (D).

Table 3
DEF values for HeLa cells irradiated with 290 MeV/u carbon ions beam (LETd = 50 keV/μm) in normoxic and hypoxic conditions for cells loaded with GemMP or GemMP-loaded nanoMOFs.

DEF (SF=10 %)	Normoxic (pO_2 = 20 %)	Hypoxic (pO_2 = 0.5 %)
GemMP	1.4	1.5
GemMP-loaded nanoMOFs	1.4	1.6

Table 4
DEF values for HeLa cells loaded with GemMP or Gem-loaded nanoMOFs and irradiated with 150 MeV/u Helium ions beam (LET_d = 12 keV/μm) in normoxic or hypoxic conditions.

DEF (SF=10 %)	Normoxic (pO_2 = 20 %)	Hypoxic (pO_2 = 0.5 %)
GemMP	1.3	1.6
GemMP-loaded nanoMOFs	1.4	1.7

helium ions (comparison of data not shown – see supplementary), which confirms the increase of radio-toxicity with the incident beam LET.

The isobologram analysis (Fig. 5) shows that, the effect of free GemMP is antagonist at low dose (1 Gy), additive at 2 Gy and synergetic for doses > 1 Gy. With GemMP encapsulated in nanoMOFs, the effect is additive at the dose of 1 Gy and synergistic for doses > 1.

Moreover, the synergistic effects of the two nanoagents are observed at higher doses for helium ions than for carbon ions (for free GemMP: above 2 Gy with helium ions and 1 Gy with carbon ions; for GemMP-loaded nanoMOFs): above 1 Gy with helium ions).

4.5. Impact of nanoMOFs, GemMP and GemMP-loaded nanoMOFs on radiation effects – impact of the extracellular matrix (3D cell cultures)

The survival curves of HeLa cultivated in 3D-CCMs and exposed to different conditions (w/o nanoagents) and irradiated with carbon and helium ions (in normoxic conditions) are provided in Fig. 6.

In line with the 2D experiments, the presence of loaded-free nanoMOFs do not influence radio-toxicity of the two irradiation beams.

Interestingly, for the two irradiation beams, the survival curves obtained with free GemMP (red) and GemMP-loaded nanoMOFs (black) are significantly different (p values of 10^{-4} (carbon) and 3.10^{-4} (helium)). DEF values(see Table 5) increased from 1.1 to 1.4 (carbon) and from 1.1 to 1.3 (helium) when the GemMP is encapsulated. It shows that, unlike the results obtained with monolayer cultures (see section 4.4.1 and 4.4.2), the effect of the agents on the radio-toxicity is affected by the presence of the ECM.

5. Discussion

This study aimed to evaluate the efficiency of combining GemMP-loaded nanoMOFs with particle therapy to treat normoxic as well as hypoxic radioresistant tumors. The effect of oxygen on radiation therapies is well documented in the literature: in normoxic conditions, after irradiation, the production of superoxide radicals $O_2^{\cdot-}$ – known to be very reactive towards biological components – causes severe toxicity (Baldacchino et al., 2019). O_2 can also directly react with the biomolecules, fixing lesions by the formation of peroxydized species making the cell damage non-repairable and permanent(Scifoni et al., 2013).

A-

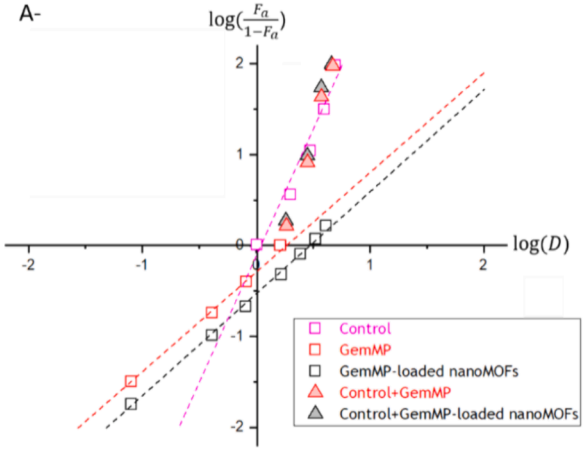

B-

Isobologram fit parameters	Dm	m
Control	1.10 (Gy)	2.75 ± 0.32
GemMP	1.79 (µg/ml)	1.12 ± 0.02
GemMP-loaded nanoMOFs	2.89 (µg/ml of GemMP) 57.8 (µg/ml of nanoMOFs)	1.11 ± 0.03

	Combination index - CI values	
Dose of carbon radiations (Gy)	GemMP	GemMP-loaded nanoMOFs
1	1.0	0.9
2	0.9	0.8
3	0.7	0.6
4	0.7	0.7

Fig. 3. (A) Graphical representation of Fa. (B) Isobologram analysis with calculated values of Dm for the treatment by 290 MeV/u carbon ions of cells: free of agents (control, data in magenta), in the presence of GemMP (data in red) or GemMP-loaded nanoMOFs (data in black). Calculated values of CI.

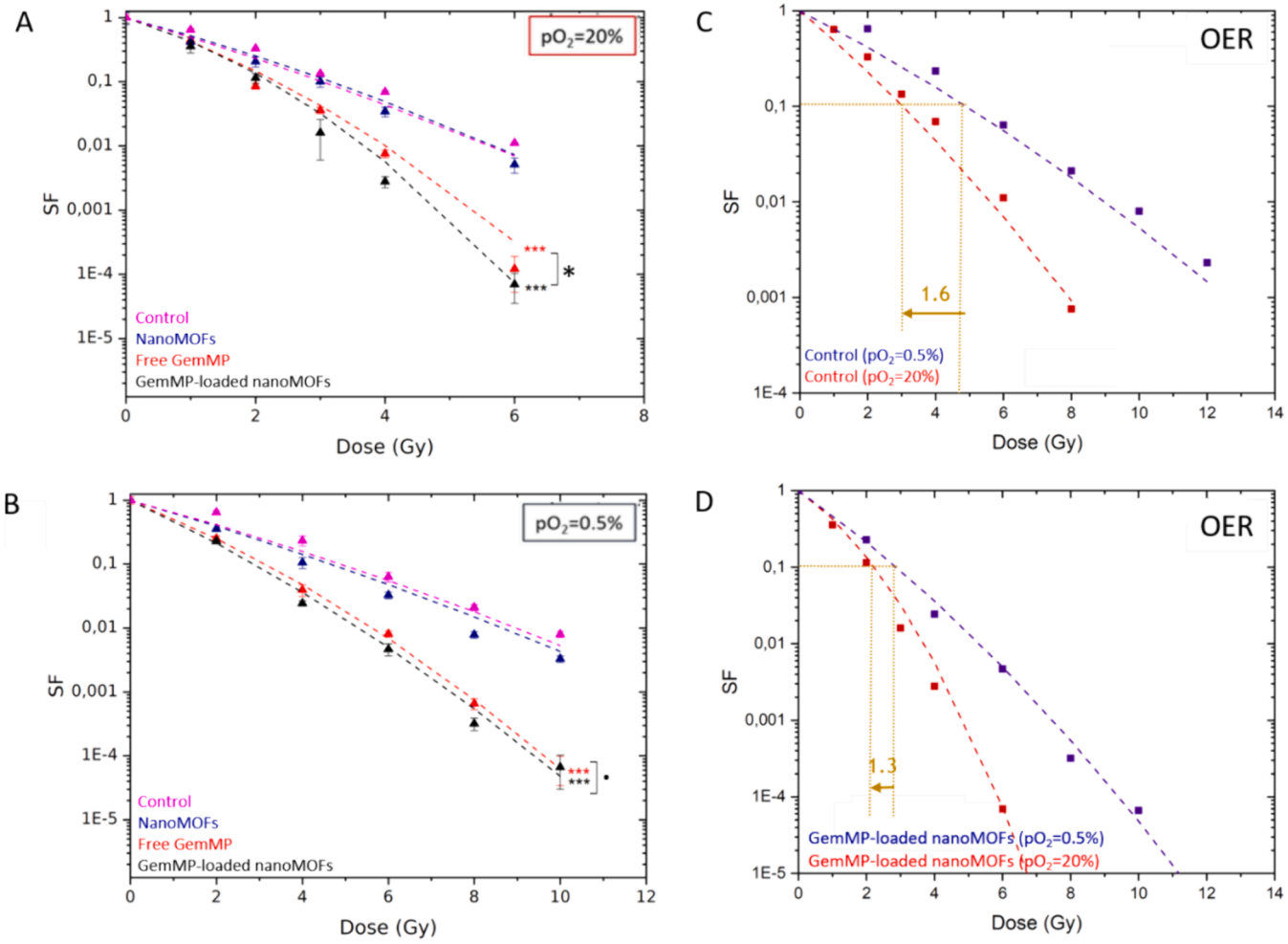

Fig. 4. Survival curves obtained with 150 MeV/u Helium ions beam (LETd = 12 keV/µm) in (A) normoxic and (B) hypoxic conditions. Differences between the control and GemMP or GemMP-loaded nanoMOFs are significant (p values < 0.001 (***)), but not significant between GemMP and GemMP-loaded nanoMOFs (p value < 0.05 (*) for normoxic and < 0.1 (.) for hypoxic conditions). Oxygen effect for control cells (C) or cells incubated with GemMP-loaded nanoMOFs (D).

When O_2 concentration is reduced (hypoxic conditions), the production of $O_2^{\cdot-}$ and the fixation of biomolecular damage decrease, thus enhancing the competitive interaction of biomolecule radicals with radical-reducing species and resulting in "chemical repair" of damage (Furusawa et al., 2000). These phenomena explain the challenge of treating hypoxic tumors.

Here, we demonstrated that the presence of GemMP-nanoMOFs enhances the deleterious effect of radiation (carbon and helium), both in normoxic and hypoxic conditions. In the presence of GemMP-loaded nanoMOFs, the dose can be reduced 1.4-fold in normoxia and at least

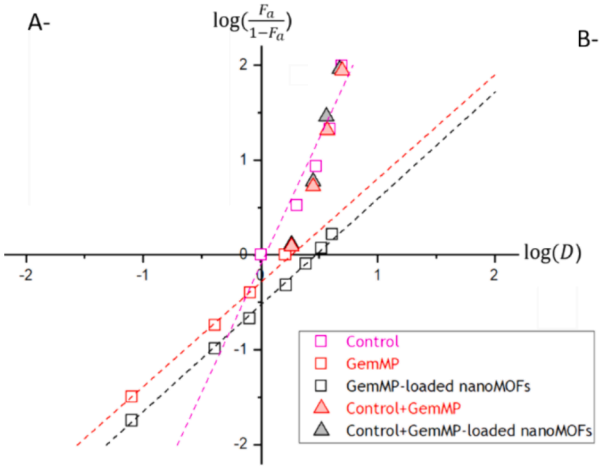

B-

Isobologram fit parameters	Dm	m
Control	1.12 (Gy)	2.64 ± 0.43
GemMP	1.79 (µg/ml)	1.12 ± 0.02
GemMP-loaded nanoMOFs	2.89 (µg/ml of GemMP) 57.8 (µg/ml of nanoMOFs)	1.11 ± 0.03

	Combination index - CI values	
Dose of helium radiations (Gy)	GemMP	GemMP-loaded nanoMOFs
1	1.1	1
2	1	0.9
3	0.8	0.7
4	0.6	0.6

Fig. 5. (A) Graphical representation of Fa. (B) Isobologram analysis with calculated values of Dm for the treatment by 150 MeV/u helium ions of cells: free of agents (control, data in magenta), in the presence of GemMP (data in red) or GemMP-loaded nanoMOFs (data in black). Calculated values of CI.

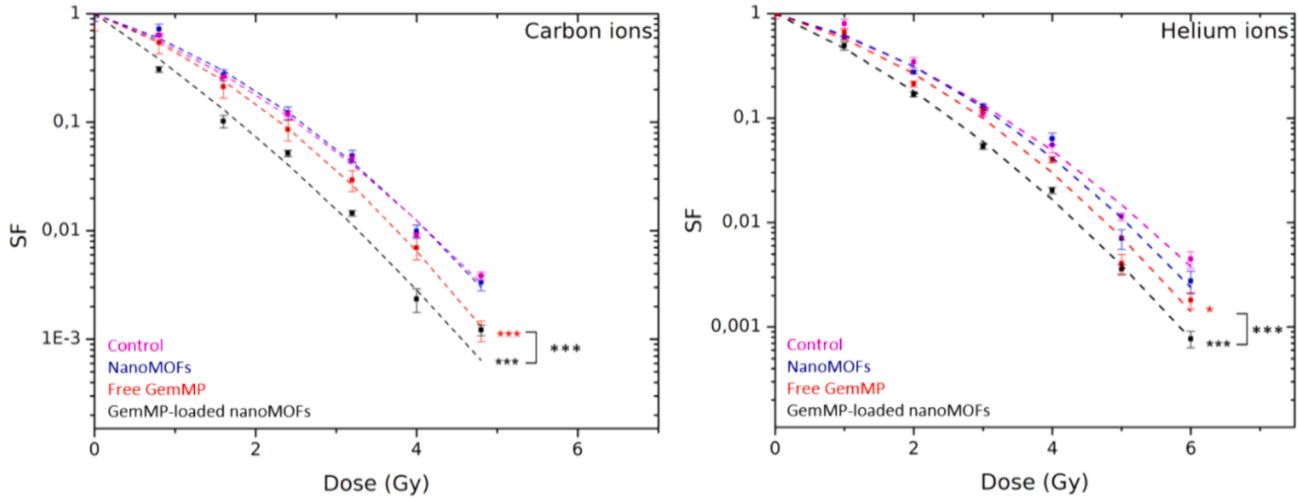

Fig. 6. Survival curves of Hela cells extracted from 3D-CCMs after exposure of 3D-CCMs to nanoMOFs (blue), free GemMP (red) and GemMP-loaded nanoMOFs (black) (control without agents in magenta), and irradiated with (A) 290 MeV/u Carbon ions and (B) 150 MeV/u Helium ions. Differences between the control and GemMP are significant for carbon (p values < 0.001 (***)) and helium ions (p values < 0.05 (*)). Differences between the control and GemMP-loaded nanoMOFs are significant (p values < 0.001 (***)) for carbon and helium ions. Differences are significant between GemMP and GemMP-loaded nanoMOFs (p value < 0.001 (***)) for the two beams.

Table 5
DEF values for 3D-CCM HeLa cells irradiated with 290 MeV/u Carbon ions (LET_d = 12 keV/µm) or 150 MeV/u Helium ions (LET_d = 50 keV/µm) in normoxic conditions for cells loaded with GemMP or Gem-loaded nanoMOFs.

DEF (SF=10 %)	Carbon	Helium
GemMP	1.1	1.1
GemMP-loaded nanoMOFs	1.4	1.3

1.6-fold in hypoxia to achieve the same cytotoxic effect (SF=10 %) than with irradiation alone. The presence of the nanoagent reduces the oxygen dependence of the cell radio-sensitization, by 14 % (carbon) and 19 % (helium) ions.

As expected, the radiotoxicity was found systematically higher for high LET radiation (carbon ions (50 keV/µm)) than for helium ions (12 keV/µm). This is well explained by the increase of the ionization density along the ion track and the consecutive induction of complex biodamage and cell killing efficiency(Hirayama et al., 2009). Consequently, because of the high lethality of these lesions, the radio-toxicity of high LET radiation is less sensitive to the presence of molecular oxygen, and the oxygen fixation mechanisms plays a minor role (OER tends to 1) (Hirayama et al., 2005; Hirayama et al., 2009). In addition, the increase of the ionization density in the track at high LET induces a drop in the radical concentration due to their recombination into molecular species (Ito et al., 2006; LaVerne, 2000). Thus, the component of indirect damage in cell killing (beta) is drastically reduced, as well as the dependence on oxygen concentration(Scifoni et al., 2013).

From a medical point of view, the resulting high relative biological effectiveness and low dependence on the O_2 concentration make heavy ion beams a modality superior to conventional radiotherapy to treat hypoxic tumors. Their physical characteristics such as a finite beam range and their dosimetric advantages are now well understood, explaining why the use of particle therapies in cancer treatment continues to expand, with carbon and helium ions as leading therapies. Carbon ions benefit from a clinical advantage over helium, as numerous studies have already been published showing their efficacy for most malignant tumors(Malouff et al., 2020). Nevertheless, helium ions exhibit intermediate physical and radiobiological properties between protons and carbon ion beams, in terms of linear energy transfer (LET), biological efficacy (RBE) and targeting (sharp lateral penumbra)

(Mairani et al., 2022). They even have advantages over carbon ions, namely reduced radiobiological uncertainties and less neutron dose. Moreover, helium ions open up new perspectives for imaging and treatment monitoring, reducing imaging dose (with comparable image quality) compared to carbon ions(Mazzucconi et al., 2018; Volz et al., 2020). Last but not least, treatment with helium ions is also interesting for its economic aspects since the technical effort needed to accelerate helium ions is less compared to carbon ions and deliverable with a cyclotron. They may provide a "streamlined economic steppingstone towards an era of widespread use of different particle species in light and heavy ion therapy" (Mairani et al., 2022).

In this context, the addition of GemMP-loaded nanoMOFs could further boost the performance of helium ions beyond that of carbon ions, in particular to overcome the radioresistance of hypoxic tumors.

After demonstrating that GemMP-loaded nanoMOFs could counteract the effects of oxygenation, the second objective was to characterize the influence of the microenvironment. We showed that these NPs are able to diffuse through the ECM (collagen matrix) and penetrate cancer cells. They are found in the cytoplasm, suggesting internalisation in the cells by endocytic process, which agrees with other works with NPs of this size (~200 nm) (Meng et al., 2016). When released in cell, GemMP may exert its intracellular cytotoxic action as reported in the literature(Li, Salzano, et al., 2020): (i) inhibition of DNA synthesis and post radiation damage repair (ii) incorporation into DNA as fraudulent base, making the defect significantly more difficult to repair (iii) interference with the cell cycle arresting in the most radio-sensitive phase (Herscher et al., 1999; Seiwert et al., 2007; Shewach and Lawrence, 1996). The cytotoxic effects of the drug cumulated with the induction of complex damage by the ions, explains the remarkable efficacy (+55 % for carbon ions and + 45 % for helium ions at 2 Gy, whatever the oxygenation degree). It is even greater than the already reported effect of other metallic NPs combined with ions. For example, for gold NPs (0.5 mmol/L), under identical hypoxia conditions (pO_2 = 0.5 %), $DEF_{SF=10\%}$ of 1.05 and 1.26 were reported for monolayer cultures irradiated with the same carbon and helium ion beams (versus 1.63 and 1.70 in our study)(Bolsa Ferruz, 2017).

Toxicity results based on 3D cell models showed that the selected working concentration of nanoagents was compatible with *in vitro* experiments (ISO 10993–5:2009-Part 5). Nevertheless, the variability reflected in the error bars makes it challenging to determine statistical significance and draw definitive conclusions about the differences in toxicity between GemMP-loaded nanoMOFs and free GemMP. However, while the radio-sensitization experiments carried out in 2D showed similar efficiencies between the free GemMP and the GemMP encapsulated in nanoMOFs, a significant difference was observed in 3D. In this case, free GemMP interact with the ECM, which decreases its penetration in cells compared to the 2D sample. The "Trojan horses" property of the nanoMOFs is thus more significant in 3D as in 2D samples. Thus, the radiosensitivity was found higher with 3D-CCM. GemMP-loaded nanoMOFs showed a greater effect than with metallic gadolinium nanoparticles for example. With the same 3D cell models, with the same carbon ions beam, the $DEF_{SF=10\%}$ was 1.06 (compared with 1.4 in this study). To the best of our knowledge, this is the first time that the efficacy of a drug delivery system combined with a particle beam has been studied and demonstrates the promising potential of such a combination to treat tumors.

While recognizing the limitations of the *in vitro* models used in this study, they provided an essential first step in evaluating the effectiveness of the strategy. They allowed precise control of hypoxia and drug delivery, offering key insights into the interactions between GemMP, nanoMOFs, and radiation. The promising *in vitro* results establish a strong foundation for future *in vivo* studies, ensuring that these more complex investigations are both ethically guided and better informed.

6. Conclusions

The multimodal approach proposed in this study aims at combining particle therapy and chemotherapy to advance cancer treatment. We demonstrated the significant potential of GemMP-loaded nanoMOFs to improve local tumor control while minimizing toxicity to healthy tissues. Notably, this nanoagent effectively enhances the impact of radiation under both normoxic and hypoxic conditions, with comparable efficiencies. We also showed that nanoMOFs successfully deliver nearly 100 % of the drug to cancer cells, even in the presence of a microenvironment. The nanoagents' ability to diffuse into tissues and maintain efficacy under hypoxic conditions highlights their potential. These encouraging outcomes and lack of obstacle bring the research closer to *in vivo* application, opening new avenues for the treatment of hypoxic tumors, which remain a major therapeutic challenge.

Funding

We acknowledge support from the Université Paris Saclay : the Interdisciplinary Centre iNanoTheRad and the 'Fédération de Chimie Physique' of Paris Saclay (CPPS). This work received support from the French National Research Agency (ANR-20-CE19-0020) and by Labex NanoSaclay (ANR-10-LABX-0035). Multiphoton imaging at LOB was supported by the Agence Nationale de la Recherche (contracts ANR-11-EQPX-0029 Morphoscope2 and ANR-10-INBS-04FBI). We thank the HIMAC synchrotron crews at QST for their excellent help during the irradiation procedures. This work is alos supported by the Research Project at QST-HIMAC and a part of this work was performed with the support by grant from JST ERATO (Grant No. JPMJER2102), Japan.

CRediT authorship contribution statement

Pauline Maury: Writing – original draft, Software, Methodology, Investigation, Formal analysis, Data curation. **Ryoichi Hirayama:** Resources, Investigation, Conceptualization. **Xue Li:** Resources. **Pierre Mahou:** Methodology, Investigation, Conceptualization. **Marie-Claire Schanne-Klein:** Supervision, Methodology. **Sandrine Lacombe:** Writing – review & editing, Supervision, Resources, Project administration. **Ruxandra Gref:** Writing – review & editing, Resources, Project administration. **Erika Porcel:** Writing – review & editing, Validation, Supervision, Resources, Project administration, Methodology, Investigation, Data curation, Conceptualization.

Declaration of competing interest

The authors declare that they have no known competing financial interests or personal relationships that could have appeared to influence the work reported in this paper.

Data availability

The data supporting this article have been included as part of the Supplementary Information.

Appendix A. Supplementary data

Supplementary data to this article can be found online at https://doi.org/10.1016/j.ijpharm.2024.124721.

References

Baati, T., Njim, L., Neffati, F., Kerkeni, A., Bouttemi, M., Gref, R., Najjar, M.F., Zakhama, A., Couvreur, P., Serre, C., Horcajada, P., 2013. In depth analysis of the in vivo toxicity of nanoparticles of porous iron(iii) metal–organic frameworks. Chem. Sci. 4 (4), 1597–1607. https://doi.org/10.1039/c3sc22116d.

Baldacchino, G., Brun, E., Denden, I., Bouhadoun, S., Roux, R., Khodja, H., 2019. Importance of radiolytic reactions during high – LET irradiation modalities : LET effect, role of O 2 and radiosensitization by nanoparticles. Cancer Nanotechnol. 1–21. https://doi.org/10.1186/s12645-019-0047-y.

Bolsa Ferruz, M., 2017. Oxygen effect in medical ion beam radiation combined with nanoparticles. Université Paris Saclay (COmUE).
Bouffard, D.Y., Laliberté, J., Momparler, R.L., 1993. Kinetic studies on 2',2'-difluorodeoxycytidine (gemcitabine) with purified human deoxycytidine kinase and cytidine deaminase. Biochem. Pharmacol. 45 (9), 1857–1861. https://doi.org/10.1016/0006-2952(93)90444-2.
Braselmann, H., Michna, A., Heß, J., Unger, K., 2015. CFAssay : statistical analysis of the colony formation assay. Radiat. Oncol. 1–6. https://doi.org/10.1186/s13014-015-0529-y.
Braselmann, H. (2019). CFAssay: Statistical analysis for the Colony Formation Assay. doi: 10.18129/B9.bioc.CFAssay.
Brown, J.M., Wilson, W.R., 2004. Exploiting tumour hypoxia in cancer treatment. Nat. Rev. Cancer 4 (6), 437–447. https://doi.org/10.1038/nrc1367.
Carmichael, J., Possinger, K., Phillip, P., Beykirch, M., Kerr, H., Walling, J., Harris, A.L., 1995. Advanced breast cancer: A phase II trial with gemcitabine. J. Clin. Oncol. 13 (11), 2731–2736. https://doi.org/10.1200/JCO.1995.13.11.2731.
Chou, T.C., 2010. Drug combination studies and their synergy quantification using the chou-talalay method. Cancer Res. 70 (2), 440–446. https://doi.org/10.1158/0008-5472.CAN-09-1947.
Chou, T.C., Martin, N., 2005. PC Software and User's Guide: A Computer Program for Quantitation of Synergism and Antagonism in Drug Combinations, and the Determination of IC50 and ED50 and LD50 Values. ComboSyn Inc.
Chou, T.C., Talalay, P., 1984. Quantitative analysis of dose-effect relationships: the combined effects of multiple drugs or enzyme inhibitors. Adv. Enzyme Regul. 22 (C), 27–55. https://doi.org/10.1016/0065-2571(84)90007-4.
Ding, M., Liu, W., Gref, R., 2022. Nanoscale MOFs: From synthesis to drug delivery and theranostics applications. Adv. Drug Deliv. Rev. 190, 114496. https://doi.org/10.1016/j.addr.2022.114496.
Durante, M., Cucinotta, F.A., 2008. Heavy ion carcinogenesis and human space exploration. Nat. Rev. Cancer 8 (6), 465–472. https://doi.org/10.1038/nrc2391.
Durante, M., Orecchia, R., Loeffler, J.S., 2017. Charged-particle therapy in cancer: Clinical uses and future perspectives. Nat. Rev. Clin. Oncol. 14 (8), 483–495. https://doi.org/10.1038/nrclinonc.2017.30.
Furusawa, Y., Fukutsu, K., Aoki, M., Itsukaichi, H., Eguchi-Kasai, K., Ohara, H., Yatagai, F., Kanai, T., Ando, K., 2000. Inactivation of aerobic and hypoxic cells from three different cell lines by accelerated 3He-, 12C- and 20Ne-Ion beams. Radiat. Res. 154 (5), 485–496. https://doi.org/10.1667/0033-7587(2000)154[0485:IOAAHC]2.0.CO;2.
Goodman, T.T., Olive, P.L., Pun, S.H., 2007. Increased nanoparticle penetration in collagenase-treated multicellular spheroids. Int. J. Nanomed. 2 (2), 265–274. http://www.ncbi.nlm.nih.gov/pubmed/17722554%0Ahttp://www.pubmedcentral.nih.gov/articlerender.fcgi?artid=PMC2673974.
Gordon Steel, G., Peckham, M.J., 1979. Exploitable mechanisms in combined radiotherapy-chemotherapy: The concept of additivity. Int. J. Radiat. Oncol. Biol. Phys. 5 (1), 85–91. https://doi.org/10.1016/0360-3016(79)90044-0.
Graeff, C., Weber, U., Schuy, C., Saito, N., Volz, L., Piersimoni, P., Seco, J., Kraemer, M., 2018. [OA027] Helium as a range probe in carbon ion therapy. Phys. Med. 52, 11. https://doi.org/10.1016/j.ejmp.2018.06.099.
Hagiwara, Y., Niimi, A., Isono, M., Yamauchi, M., Yasuhara, T., Limsirichaikul, S., Oike, T., Sato, H., Held, K., Nakano, T., Shibata, A., 2017. 3D-structured illumination microscopy reveals clustered DNA double-strand break formation in widespread γH2AX foci after high LET heavy-ion particle radiation. Oncotarget 8 (65), 109370–109381. https://doi.org/10.18632/oncotarget.22679.
Hagiwara, Y., Oike, T., Niimi, A., Yamauchi, M., Sato, H., Limsirichaikul, S., Held, K., Nakano, T., Shibata, A., 2019. Clustered DNA double-strand break formation and the repair pathway following heavy-ion irradiation. J. Radiat. Res. 60 (1), 69–79. https://doi.org/10.1093/jrr/rry096.
Herscher, L.L., Cook, J.A., Pacelli, R., Pass, H.I., Russo, A., Mitchell, J.B., 1999. Principles of chemoradiation: theoretical and practical considerations. Oncology (Williston Park) 13 (10 Suppl 5), 11–22. http://www.ncbi.nlm.nih.gov/pubmed/10550823.
Hirayama, R., Furusawa, Y., Fukawa, T., Ando, K., 2005. Repair Kinetics of DNA-DSB Induced by X-rays or Carbon Ions under Oxic and Hypoxic Conditions. J. Radiat. Res. 46 (3), 325–332. https://doi.org/10.1269/jrr.46.325.
Hirayama, R., Ito, A., Tomita, M., Tsukada, T., Yatagai, F., Noguchi, M., Matsumoto, Y., Kase, Y., Ando, K., Okayasu, R., Furusawa, Y., 2009. Contributions of Direct and Indirect Actions in Cell Killing by High-LET Radiations. Radiat. Res. 171 (2), 212–218. https://doi.org/10.1667/RR1490.1.
Horcajada, P., Chalati, T., Serre, C., Gillet, B., Sebrie, C., Baati, T., Eubank, J.F., Heurtaux, D., Clayette, P., Kreuz, C., Chang, J.S., Hwang, Y.K., Marsaud, V., Bories, P.N., Cynober, L., Gil, S., Férey, G., Couvreur, P., Gref, R., 2010. Porous metal-organic-framework nanoscale carriers as a potential platform for drug deliveryand imaging. Nat. Mater. 9 (2), 172–178. https://doi.org/10.1038/nmat2608.
Huang, R.Y., Pei, L., Liu, Q., Chen, S., Dou, H., Shu, G., Yuan, Z.X., Lin, J., Peng, G., Zhang, W., Fu, H., 2019. Isobologram analysis: A comprehensive review of methodology and current research. Front. Pharmacol. 10 (OCT), 1–12. https://doi.org/10.3389/fphar.2019.01222.
Ito, A., Nakano, H., Kusano, Y., Hirayama, R., Furusawa, Y., Murayama, C., Mori, T., Katsumura, Y., Shinohara, K., 2006. Contribution of Indirect Action to Radiation-Induced Mammalian Cell Inactivation: Dependence on Photon Energy and Heavy-Ion LET. Radiat. Res. 165 (6), 703–712. https://doi.org/10.1667/RR3557.1.
Jain, R.K., 1997. Delivery of molecular and cellular medicine to solid tumors. Adv. Drug Deliv. Rev. 26 (2–3), 71–90. https://doi.org/10.1016/S0169-409X(97)00027-6.
LaVerne, J.A., 2000. Track effects of heavy ions in liquid water. Radiat. Res. 153 (5 Pt 1), 487–496.
Li, M., Zhang, Y., Zhang, Q., and Li, J. (2022). Tumor extracellular matrix modulating strategies for enhanced antitumor therapy of nanomedicines. In: Materials Today Bio (Vol. 16). Elsevier B.V. doi: 10.1016/j.mtbio.2022.100364.
Li, X., Lachmanski, L., Safi, S., Sene, S., Serre, C., Grenèche, J.M., Zhang, J., Gref, R., 2017. New insights into the degradation mechanism of metal-organic frameworks drug carriers. Sci. Rep. 7 (1), 1–11. https://doi.org/10.1038/s41598-017-13323-1.
Li, X., Porcel, E., Menendez-Miranda, M., Qiu, J., Yang, X., Serre, C., Pastor, A., Desmaële, D., Lacombe, S., Gref, R., 2020a. Highly Porous Hybrid Metal-Organic Nanoparticles Loaded with Gemcitabine Monophosphate: a Multimodal Approach to Improve Chemo- and Radiotherapy. ChemMedChem 15 (3), 274–283. https://doi.org/10.1002/cmdc.201900596.
Li, X., Salzano, G., Qiu, J., Menard, M., Berg, K., Theodossiou, T., Ladavière, C., Gref, R., 2020b. Drug-Loaded Lipid-Coated Hybrid Organic-Inorganic "Stealth" Nanoparticles for Cancer Therapy. Front. Bioeng. Biotechnol. 8. https://doi.org/10.3389/fbioe.2020.01027.
Lorat, Y., Brunner, C., Schanz, S., Jakob, B., Taucher-Scholz, G., Rübe, C., 2015. Nanoscale analysis of clustered DNA damage after high-LET irradiation by quantitative electron microscopy - The heavy burden to repair. DNA Repair 28, 93–106. https://doi.org/10.1016/j.dnarep.2015.01.007.
Magzoub, M., Jin, S., Verkman, A.S., 2008. Enhanced macromolecule diffusion deep in tumors after enzymatic digestion of extracellular matrix collagen and its associated proteoglycan decorin. FASEB J. 22 (1), 276–284. https://doi.org/10.1096/fj.07-9150com.
Mairani, A., Mein, S., Blakely, E., Debus, J., Durante, M., Ferrari, A., Fuchs, H., Georg, D., Grosshans, D.R., Guan, F., Haberer, T., Harrabi, S., Horst, F., Inaniwa, T., Karger, C. P., Mohan, R., Paganetti, H., Parodi, K., Sala, P., Weber, U., 2022. Roadmap: Helium ion therapy. Phys. Med. Biol. 67 (15). https://doi.org/10.1088/1361-6560/ac65d3.
Malouff, T.D., Mahajan, A., Krishnan, S., Beltran, C., Seneviratne, D.S., & Trifiletti, D.M. (2020). Carbon Ion Therapy: A Modern Review of an Emerging Technology. In: Frontiers in Oncology (Vol. 10). Frontiers Media S.A. doi: 10.3389/fonc.2020.00082.
Maury, P., Porcel, E., Mau, A., Lux, F., Tillement, O., Mahou, P., Schanne-Klein, M.-C., Lacombe, S., 2021. Rapid evaluation of novel therapeutic strategies using a 3D collagen-based tissue-like model. Front. Bioeng. Biotechnol. https://doi.org/10.3389/fbioe.2021.574035.
Mazzucconi, D., Agosteo, S., Ferrarini, M., Fontana, L., Lante, V., Pullia, M., Savazzi, S., 2018. Mixed particle beam for simultaneous treatment and online range verification in carbon ion therapy: Proof-of-concept study. Med. Phys. 45 (11), 5234–5243. https://doi.org/10.1002/mp.13219.
McKeown, S.R., 2014. Defining normoxia, physoxia and hypoxia in tumours—implications for treatment response. Br. J. Radiol. 87 (1035), 20130676. https://doi.org/10.1259/bjr.20130676.
Meng, W., Garnett, M.C., Walker, D.A., Parker, T.L., 2016. Penetration and intracellular uptake of poly(glycerol-adipate) nanoparticles into three-dimensional brain tumour cell culture models. Exp. Biol. Med. 241 (5), 466–477. https://doi.org/10.1177/1535370215610441.
Minchinton, A.I., Tannock, I.F., 2006. Drug penetration in solid tumours. Nat. Rev. Cancer 6 (8), 583–592. https://doi.org/10.1038/nrc1893.
Nakano, T., Akamatsu, K., Tsuda, M., Tujimoto, A., Hirayama, R., Hiromoto, T., Tamada, T., Ide, H., Shikazono, N., 2022. Formation of clustered DNA damage in vivo upon irradiation with ionizing radiation: Visualization and analysis with atomic force microscopy. Proc. Natl. Acad. Sci. 119 (13). https://doi.org/10.1073/pnas.2119132119.
Netti, P.A., Berk, D.A., Swartz, M.A., Grodzinsky, A.J., Jain, R.K., 2000. Role of extracellular matrix assembly in interstitial transport in solid tumors. Cancer Res. 60 (9), 2497–2503.
Pauwels, B., Korst, A.E.C., de Pooter, C.M.J., Lambrechts, H.A.J., Pattyn, G.G.O., Lardon, F., Vermorken, J.B., 2003. The radiosensitising effect of gemcitabine and the influence of the rescue agent amifostine in vitro. Eur. J. Cancer 39 (6), 838–846. https://doi.org/10.1016/S0959-8049(03)00002-9.
Porcel, E., Tillement, O., Lux, F., Mowat, P., Usami, N., Kobayashi, K., Furusawa, Y., Le Sech, C., Li, S., Lacombe, S., 2014. Gadolinium-based nanoparticles to improve the hadrontherapy performances. Nanomed. Nanotechnol. Biol. Med. 10 (8), 1601–1608. https://doi.org/10.1016/j.nano.2014.05.005.
Rodriguez-Ruiz, V., Maksimenko, A., Anand, R., Monti, S., Agostoni, V., Couvreur, P., Lampropoulou, M., Yannakopoulou, K., Gref, R., 2015. Efficient "green" encapsulation of a highly hydrophilic anticancer drug in metal-organic framework nanoparticles. J. Drug Target. 23 (7–8), 759–767. https://doi.org/10.3109/1061186X.2015.1073294.
Sage, E., Shikazono, N., 2017. Radiation-induced clustered DNA lesions: Repair and mutagenesis. Free Radic. Biol. Med. 107, 125–135. https://doi.org/10.1016/j.freeradbiomed.2016.12.008.
Scifoni, E., Tinganelli, W., Weyrather, W.K., Durante, M., Maier, A., Krämer, M., 2013. Including oxygen enhancement ratio in ion beam treatment planning: Model implementation and experimental verification. Phys. Med. Biol. 58 (11), 3871–3895. https://doi.org/10.1088/0031-9155/58/11/3871.
Seiwert, T.Y., Salama, J.K., Vokes, E.E., 2007. The concurrent chemoradiation paradigm - General principles. Nat. Clin. Pract. Oncol. 4 (2), 86–100. https://doi.org/10.1038/ncponc0714.
Shewach, D.S., Lawrence, T.S., 1996. Gemcitabine and radiosensitization in human tumor cells. Invest. New Drugs 14 (3), 257–263. https://doi.org/10.1007/BF00194528.
Simon-Yarza, T., Giménez-Marqués, M., Mrimi, R., Mielcarek, A., Gref, R., Horcajada, P., Serre, C., Couvreur, P., 2017. A Smart Metal-Organic Framework Nanomaterial for Lung Targeting. Angew. Chem. Int. Ed. 56 (49), 15565–15569. https://doi.org/10.1002/anie.201707346.

Song, G., Cheng, L., Chao, Y., Yang, K., Liu, Z., 2017. Emerging Nanotechnology and Advanced Materials for Cancer Radiation Therapy. Adv. Mater. 29 (32), 1–26. https://doi.org/10.1002/adma.201700996.

Steichen, S.D., Caldorera-Moore, M., Peppas, N.A., 2013. A review of current nanoparticle and targeting moieties for the delivery of cancer therapeutics. Eur. J. Pharm. Sci. 48 (3), 416–427. https://doi.org/10.1016/j.ejps.2012.12.006.

Tchoryk, A., Taresco, V., Argent, R.H., Ashford, M., Gellert, P.R., Stolnik, S., Grabowska, A., Garnett, M.C., 2019. Penetration and uptake of nanoparticles in 3D tumor spheroids. Bioconjug. Chem. 30 (5), 1371–1384. https://doi.org/10.1021/acs.bioconjchem.9b00136.

Vaupel, P., Mayer, A., 2007. Hypoxia in cancer: Significance and impact on clinical outcome. Cancer Metastasis Rev. 26 (2), 225–239. https://doi.org/10.1007/s10555-007-9055-1.

Volz, L., Kelleter, L., Brons, S., Burigo, L., Graeff, C., Niebuhr, N.I., Radogna, R., Scheloske, S., Schömers, C., Jolly, S., Seco, J., 2020. Experimental exploration of a mixed helium/carbon beam for online treatment monitoring in carbon ion beam therapy. Phys. Med. Biol. 65 (5), 055002. https://doi.org/10.1088/1361-6560/ab6e52.

Wuttke, S., Braig, S., Preiß, T., Zimpel, A., Sicklinger, J., Bellomo, C., Rädler, J.O., Vollmar, A.M., Bein, T., 2015. MOF nanoparticles coated by lipid bilayers and their uptake by cancer cells. Chem. Commun. 51 (87), 15752–15755. https://doi.org/10.1039/c5cc06767g.